Instrument-Based Noncontact Doppler Radar Vital Sign Detection System Using Heterodyne Digital Quadrature Demodulation Architecture

Changzhan Gu, *Student Member, IEEE*, Changzhi Li, *Student Member, IEEE*, Jenshan Lin, *Senior Member, IEEE*, Jiang Long, Jiangtao Huangfu, and Lixin Ran

***Abstract*—In this paper, we present a fast solution to build a Doppler radar system for noncontact vital sign detection (VSD) using instruments that are generally equipped in radio-frequency and communication laboratories. This paper demonstrates the feasibility of conducting research on VSD in ordinary radio-frequency laboratories. The system is designed with a heterodyne digital quadrature demodulation architecture that helps mitigate quadrature channel imbalance and eliminate the complicated dc offset calibration required for arctangent demodulation. Moreover, its tunable carrier frequency helps select different optimal frequencies for different human objects. Two sets of extensive experiments have been carried out in the laboratory environment with a self-designed 2.4-GHz patch antenna array and a 1–18-GHz broadband antenna. The test results are satisfactory: for a 0-dBm transmit power, the detection range can be extended to 2.5 m with accuracy higher than 80%. The system is also capable of detecting vital signs in the presence of different obstructions between the subject and the antenna.**

***Index Terms*—Digital quadrature demodulation, Doppler radar, heartbeat, instruments, life detection, noncontact detection, remote sensing, respiration, software radio, variable-carrier-frequency test, vital sign.**

I. Introduction

THE FIRST effort to sense physiological movements using microwave Doppler radar dates back to the early 1970s [1]. Since then, many experiments and improvements in detection systems have been reported. An X-band microwave life-detection system was built in 1980 [2], and two other systems working in the L- and the S-bands were built for searching human subjects under earthquake rubbles or behind a barrier [3]. It is believed that there will be a growing market for appliances that allow noncontact detection of vital signs such as heartbeat and respiration [4]. A direct-conversion microwave Doppler radar system and a radar system with a frequency-tuning technique were recently introduced in [5] and [6], which are custom-built systems for specific applications of noncontact vital sign detection (VSD).

One might think that noncontact VSD radar systems must consist of complicated and rigid RF circuitry, since the very weak vital signs seem unable to be acquired by a general-purpose radar architecture. The recently reported VSD radar systems, as aforementioned, are all custom-built systems, which may be time consuming and cost inefficient for some research institutes. Moreover, rigorous technical considerations have to be taken into account for each specific radar system, which limits the conduction of research on VSD. For example, the microprocessor-controlled clutter-cancellation system in [3] and the dc offset compensation unit in [4] add to the system complexity, making the measurement inconvenient. The construction of radar systems in [5] and [6] must take considerable time and labor. Many laboratories have to spend significant time and effort to design and build the radar system before they could actually conduct measurements to analyze the results. However, part of the research on noncontact VSD may focus on advanced signal processing and analysis techniques rather than the detection system itself. For example, the research on biometric identification by distinguishing an individual's radar vital sign signal carrying physiological and cardiopulmonary signatures has strong focus on signal processing and analysis; thus, a detection system that can quickly be assembled would accelerate such research.

In this paper, we present a solution to build a Doppler radar system for noncontact VSD in a short period of time. The radar system is built from general-purpose RF and communication instruments that are widely used and equipped in RF/microwave laboratories. The system is straightforward to build by connecting the instruments and can quickly be disassembled for other applications. No extra RF/microwave components and modules are needed, neither is printed-circuit-board or integrated-chip design required, enabling many RF/microwave laboratories to participate in VSD research. The system, which is easily

Manuscript received April 29, 2009; revised June 26, 2009. First published October 6, 2009; current version published May 12, 2010. This work was supported in part by the National Science Foundation of China under Grant 60671003, by the 863 Project under Grant 2009AA01Z227, by the Zhejiang Province Natural Science Foundation of China (ZJNSF) under Grant R105253 and Grant Y1080715, by the NCET-07-0750, and by the Ph.D. Program Foundation of the Ministry of Education of China under Grant 20070335120. The Associate Editor coordinating the review process for this paper was Dr. Devendra Misra.

C. Gu was with the Department of Information and Electronic Engineering, Zhejiang University, Hangzhou 310027, China. He is now with the Department of Electrical and Computer Engineering, University of Florida, Gainesville, FL 32611 USA (e-mail: gucz@zju.edu.cn; gucz@ufl.edu).

C. Li is with the Department of Electrical and Computer Engineering, Texas Tech University, Lubbock, TX 79409 USA (e-mail: changzhi@ufl.edu).

J. Lin is with the Department of Electrical and Computer Engineering, University of Florida, Gainesville, FL 32611 USA (e-mail: jenshan@ufl.edu).

J. Long, J. Huangfu, and L. Ran are with the Department of Information and Electronic Engineering, Zhejiang University, Hangzhou 310027, China (e-mail: longj@zju.edu.cn; huangfujt@zju.edu.cn; ranlx@zju.edu.cn).

Color versions of one or more of the figures in this paper are available online at http://ieeexplore.ieee.org.

Digital Object Identifier 10.1109/TIM.2009.2028208

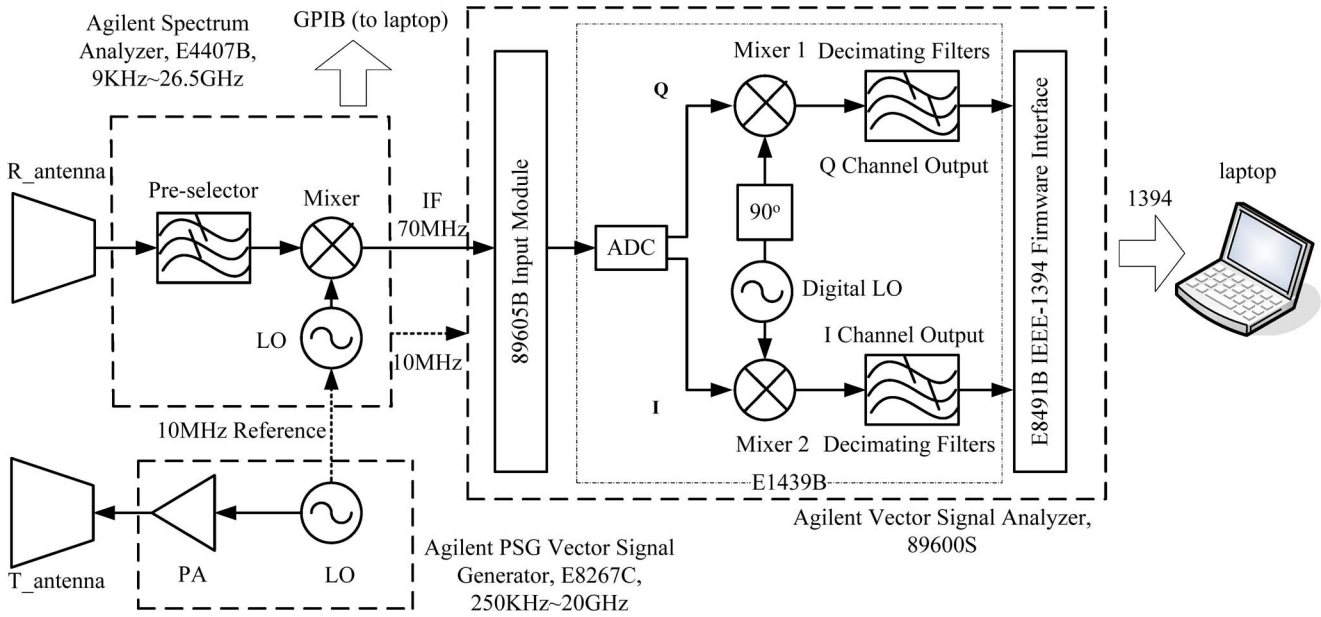

Fig. 1. Block diagram of the instrument-based radar system.

configurable and very reliable, is convenient for conducting system-level testing in the early stage of research to acquire vital sign data and can be the fundamental element for further research.

The instrument-based radar system, which is built in reconfigurable radio architecture with a digital I/Q demodulation technique, includes the following instrument components: Agilent spectrum analyzer E4407B, Agilent vector signal generator E8267C, and Agilent vector signal analyzer 89600S. These instruments or equivalent models are standard test equipment. Moreover, the assembled system has demonstrated some advantages over previously reported systems.

To the knowledge of the authors, it is the first reported VSD system with a digital I/Q demodulation technique that mitigates I/Q mismatch occurring in the analog quadrature downconverter architecture [9] and eliminates the complicated dc offset calibration required for arctangent demodulation [4]. The instrument-based system is a tunable system in which the carrier frequency could be tuned from the UHF band to the K-band. In contrast to custom-built single-frequency systems, the instrument-based system is tunable in a very wide frequency range to allow electromagnetic waves to penetrate through different depths of obstacles, which is very useful for the research of radar-based earthquake rescue techniques. Moreover, according to the discussion in [11] on the optimal carrier frequency in a rigorous nonlinear phase modulation analysis, there exist different optimal carrier frequencies for different people with different physiological movement amplitudes. Therefore, the instrument-based system is beneficial in this application. The system is also potentially capable of detecting multiple subjects using a multiple-input–multiple-output technique [15].

The system configuration and setup are shown in Section II. In Section III, the system operation and performance are analyzed. The measurement results are presented in Section IV. Finally, a conclusion is given in Section V.

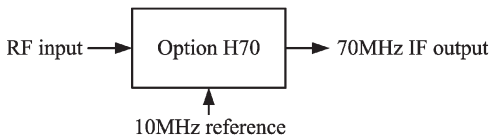

Fig. 2. Functional diagram of the downconversion module Option H70.

II. Instrument-Based Radar System

The simplified block diagram of the instrument-based radar system is illustrated in Fig. 1. The radar transceiver consists of three instruments, i.e., Agilent spectrum analyzer E4407B, Agilent vector signal generator E8267C, and Agilent vector signal analyzer 89600S.

The design of the transmitter chain is straightforward. The transmit antenna is connected to the Agilent vector signal generator E8267C, which acts as the source with a frequency-tuning range of up to 20 GHz. With the appropriate setup, the signal generator is able to output microwave signals with different frequencies, and the transmitted power can also independently be changed. In the block diagram, the signal generator is simplified as a local oscillator (LO), which generates signal stable in phase and amplitude, and a power amplifier (PA), which amplifies the LO signal to the required power level. A 10-MHz reference signal is generated as the clock for the whole system, so that all the components in the transceiver are synchronized. Therefore, coherent demodulation is achieved. The receiver chain consists of two parts: the RF front end and the intermediate-frequency (IF) downconverter. The reflected microwave signal, which is modulated by vital signs, is received by the antenna and sent into the spectrum analyzer that downconverts the microwave signal to the 70-MHz IF output. This process is realized by the internal module Option H70 of E4407B, which is illustrated in Fig. 2. H70 automatically downconverts RF input to 70-MHz output as long as the RF signal is lower than 26.5 GHz.

The IF signal is then fed to the 89600S. The preselector shown in the dashed box in Fig. 1 has a tunable filter to reject out-of-band interference that would create unwanted responses at the IF. The 89600S is an instrument with cutting-edge digital processing features that provide full access to a wide range of vector-signal-analysis (VSA) capabilities in its software. Through general-purpose-interface-bus (GPIB) connection, the 89600S can control the spectrum analyzer to fulfill coherent RF-to-IF signal downconversion. The vector signal analyzer used in this experiment mainly consists of the following standard components: 89601A VSA software with Option 100 (VSA), E8491B IEEE 1394 PC link to VMEbus eXtensions for Instrumentation (VXI), C-size with Option 001 (OHCI-based IEEE 1394/PCI card), E1439 VXI 70-MHz IF digitizer, and 89605B RF input module with Option 611 (cable adapter kit). The downconverted 70-MHz IF signal is sent to the 89605B module that provides signal calibration. The digitization of the 70-MHz IF signal is carried out at the analog–digital converter (ADC) E1439, with a sampling rate of 95 MSa/S and a bandwidth of 36 MHz. It should be noted that, although not shown in Fig. 1, an antialiasing filter before digitization is applied to limit the input frequencies of the ADC to less than one-half of the sampling rate to avoid alias products.

Sampled data are stored, and digital quadrature downconversion is performed in the 89601A VSA software externally running on a computer connected to the analyzer via the IEEE1394 PC link. The technique of digital demodulation in IF leads to very high demodulation accuracy because it assures accurate matching of the I and Q channels. By appropriately setting the VSA software, microwave signals are downconverted to and digitized at 70-MHz IF and digitally demodulated to the baseband in two quadrature I/Q chains. Two decimating filters resample each chain and output digital baseband signals, which are recorded and processed in the VSA software.

The baseband digital output is filtered, windowed, and autocorrelated in the MATLAB environment. Fast Fourier transform (FFT) is applied to obtain the spectrum of the vital sign signal. Spectral analysis [10] and performance evaluation are also carried out in MATLAB.

Two types of antenna are used in the measurement. One is a 2.4-GHz microstrip patch antenna array fabricated on an FR4 substrate with a dielectric constant of 4.6 and a thickness of 1.5 mm. Two patch antenna arrays are fabricated together, with one for transmitting and the other for receiving. The total size is 459 mm $\times$ 222 mm. The antenna radiation pattern has been measured in an anechoic chamber. The maximum gain reaches 6.5 dB at 2.4 GHz, and the beamwidth is 40°. The other antenna is a commercial broadband horn antenna, i.e., HD-10180DRHA, manufactured by Hengda Microwave, Xi'an, China. The operating frequency of this broadband antenna ranges from 1 to 18 GHz, and the gain varies between 10 and 16.5 dB, depending on the frequency. The broadband antenna is used to conduct experiments at different frequencies to evaluate the system performance. Fig. 3 shows a photograph of the instrument-based system. The inset shows the layout of the designed 2.4-GHz patch antennas.

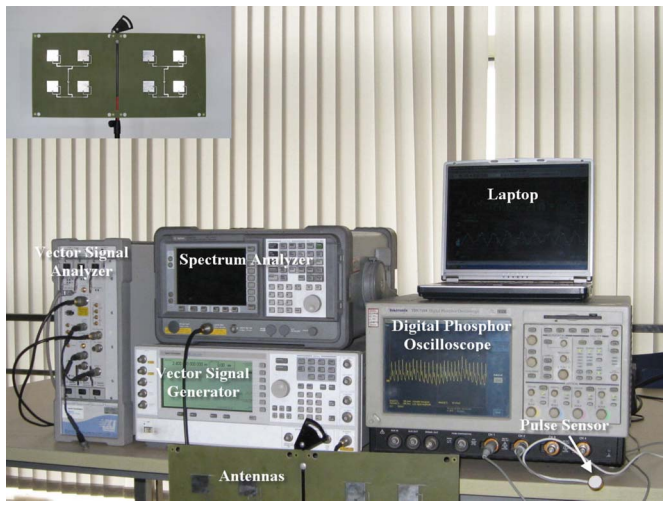

Fig. 3. Photograph of the instrument-based system for VSD. Inset: layout of the designed 2.4-GHz patch antennas.

III. System and Performance Analysis

The signal source E8267C generates a single-tone microwave signal

$$T(t) = \cos\left(2\pi f t + \phi(t)\right) \tag{1}$$

where f is the carrier frequency, t is elapsed time, and $\phi(t)$ is the phase noise of the signal source. $T(t)$ is targeted at the human chest, and its phase is modulated by the chest's periodic displacement caused by heartbeat and respiration. Therefore, the reflected microwave signal carries information of the heartbeat and respiration modulated in phase [5]. The reflected microwave signal is

$$R(t) \approx \cos\left[2\pi f t - \frac{4\pi d_0}{\lambda} - \frac{4\pi x(t)}{\lambda} + \phi\left(t - \frac{2d_0}{c}\right)\right] \tag{2}$$

where d_0 is the distance between the detection system and the target, λ is the carrier wavelength, $x(t)$ is the chest wall displacement caused by heartbeat and respiration, and $\phi(t - 2d_0/c)$ is the phase noise with time offset. $R(t)$ is received at the R_antenna and downconverted to 70-MHz IF by the Agilent spectrum analyzer E4407B Option H70. The 10-MHz reference is applied to the Option H70 to synchronize the receiver chain and the transmitter chain. After downconversion, the IF output signal is

$$R_{\mathrm{IF}}(t) \approx \cos\left[2\pi f_{\mathrm{IF}} t + \theta + \frac{4\pi x(t)}{\lambda} + \Delta\phi(t)\right] \tag{3}$$

where $f_{\mathrm{IF}} = 70\ MHz$ is the output IF, $\Delta\phi(t) = \phi(t) - \phi(t - 2d_0/c)$ is the residual phase noise, and $\theta = 4\pi d_0/\lambda + \theta_0$ is the constant phase shift determined by the distance to the target. Several other factors, e.g., the phase shift of the mixer and the antenna, contribute to the value of θ_0.

The 70-MHz IF signal is digitized by the E1439 ADC module, with a sampling rate of 95 MSa/S and a bandwidth

TABLE I
PERFORMANCE COMPARISON BETWEEN THE INSTRUMENT-BASED SYSTEM AND PREVIOUS SYSTEMS

	Detection Range [GHz]	Penetration Depth [mm]	Modulation Depth (Normalized)	I/Q Balance	DC Offset
K.M.Chen et al.	1.15	36.091	48.1711	N/A	High
	0.45	52.843	18.8494		
A. Droitcour et al.	1.6	30.366	67.0206	Imbalance	High
	2.4	22.956	100.5310		
Y.Xiao et al.	Ka band (26~40)	0.648~0.999	1089.0855~ 1675.5161	N/A	Low
C.Gu et al.	0.3~20	1.379~62.142	12.5664~ 837.7580	Balance	Low

of 36 MHz. The digitized IF output is

$$R_{\mathrm{IF}}(n) \approx \cos\left[2\pi f_{\mathrm{IF}} n + \theta + \frac{4\pi x(n)}{\lambda} + \Delta\phi(n)\right], \quad n = 1, 2, 3, \ldots \tag{4}$$

where n is the point of digitized signal series. The digital data are recorded and processed in the VSA software. Two digital LO signals, with a phase difference of $\pi/2$, are applied to the stored digital IF signal to downconvert to the baseband in two quadrature receiver paths I and Q. It is demonstrated in [5] that the I/Q demodulation helps to mitigate the null detection point problem when very weak or no signal in one of the quadrature channels occurs at certain distances. After the digital quadrature demodulation, the baseband output can be represented as

$$\mathrm{I}: \quad B_I(n) = \cos\left[\theta + \frac{4\pi x(n)}{\lambda} + \Delta\phi(n)\right], \quad n = 1, 2, 3, \ldots \tag{5}$$

$$\mathrm{Q}: \quad B_Q(n) = \cos\left[\theta - \frac{\pi}{2} + \frac{4\pi x(n)}{\lambda} + \Delta\phi(n)\right], \quad n = 1, 2, 3, \ldots. \tag{6}$$

When the displacement $x(n)$ is relatively small and θ is an odd multiple of $\pi/2$ in I or $\theta - \pi/2$ is the odd multiple of $\pi/2$ in Q, small-angle approximation is valid, and the baseband output can be approximated as

$$B(n) = \frac{4\pi x(n)}{\lambda} + \Delta\phi(n), \quad n = 1, 2, 3 \ldots. \tag{7}$$

In this case, neglecting the residual phase noise $\Delta\phi(n)$, the baseband output is proportional to the chest displacement $x(n)$ caused by the heartbeat and respiration. Displaying the baseband output would directly give vital signs summed by heartbeat, respiration, and associated residual phase noise.

The instrument-based VSD system has a wide frequency-tuning range of up to 20 GHz. It is theoretically demonstrated in the Appendix that, with such a carrier-frequency-tuning rage, a null detection point could always be tuned to an optimum detection point by changing the transmit RF. For example, if the distance between the detection system and the target is 1 m, the null point can be changed to the optimum point by tuning the carrier frequency as long as the system tuning range is larger than 75 MHz. Moreover, the proposed tunable VSD system serves well as a prototype system to explore the possibility of constructing a wide-detection-range life-detection system that can penetrate various depths of debris to search for survivors.

The proposed instrument-based VSD system is advantageous with the heterodyne (indirect conversion) architecture and digital I/Q demodulation technique. This digital architecture retains all the information and produces better results than previous analog systems [12]. For the conventional quadrature direct-conversion architecture such as the quadrature transceiver for noncontact cardiopulmonary monitoring [5], I/Q imbalance and dc offset are two inevitable challenges that degrade the demodulation accuracy and the output signal-to-noise ratio. To ensure I/Q amplitude and phase balance, complicated calibration procedures such as the Gram–Schmidt procedure have to be applied [13]. However, by using the digital I/Q demodulation technique, the two output channels are in perfect quadrature-phase relationship, making calibration procedures unnecessary. To overcome the dc offset problem, which exists in previously reported VSD system architectures [3]–[5], subsystems such as the dc offset compensation unit [4] can be applied to obtain better performance. However, these methods definitely add to the system complexity. If configured with a heterodyne architecture, there will be no significant amount of dc offset. The instrument-based system conveniently provides the function of heterodyne digital quadrature demodulation by virtue of the involved instruments' inherent capabilities.

If configured with appropriate antennas, the proposed system is able to work at lower frequencies that give larger penetration depths, which imply how deep the transmitted electromagnetic waves can penetrate to the body. A larger penetration depth usually provides a larger chest wall displacement, which, in turn, results in a larger depth of phase modulation. Table I illustrates the performance comparison between the instrument-based system and other previous systems. Phase modulation depth is defined by $4\pi x(t)/\lambda$ and is normalized by the chest wall displacement $x(t)$. The digital IF technique of the proposed system ensures the I/Q balance and the heterodyne demodulation architecture reduces the dc offset.

IV. VITAL SIGN MEASUREMENTS

The measurement setup for VSD is illustrated in Fig. 4. Breathing normally, the subject is seated to face the antenna, from a distance of d meters away. An integrated pulse sensor (HK-2000B) is wrapped around the wrist to measure the pulse signal due to heartbeat, which is digitized by TDS7104 to provide the reference signal. Three sets of measurements

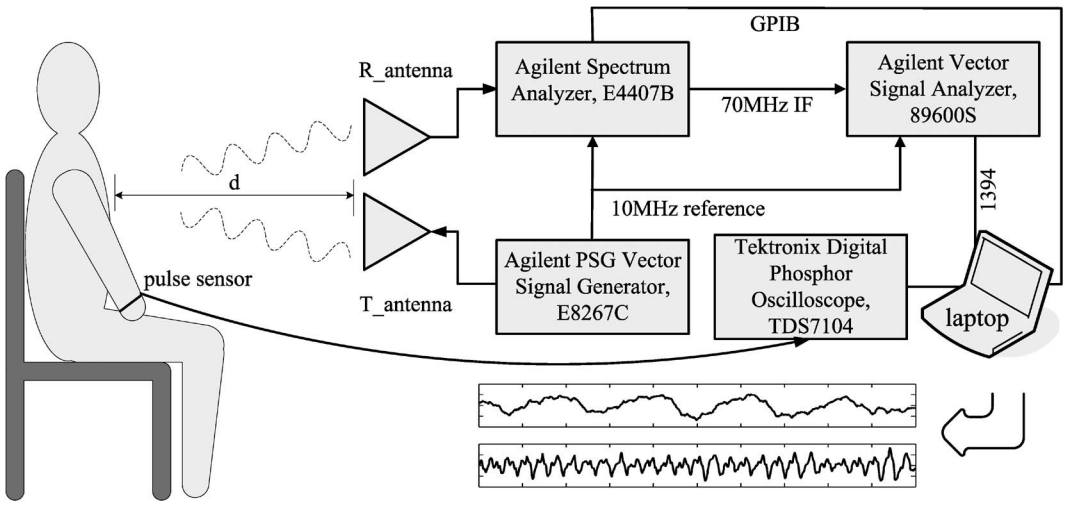

Fig. 4. Measurement setup for VSD.

were carried out. First, a 2.4-GHz printed patch antenna was designed and used to evaluate the system performance at a fixed frequency. Second, a broadband antenna HD-10180DRHA (1–18 GHz) was used to perform frequency-tuning experiments. Third, measurement experiments with various obstructions in between were carried out to investigate the system's penetration ability.

The 70-MHz IF signal is digitized by the 89600S and is processed by the VSA software installed on a PC. To obtain the respiration and heartbeat signals, further signal processing is needed. This process is performed on a MATLAB platform, which is also installed on the PC. The vital sign signal processing techniques are similar to those applied in [7]. Since the amplitude of respiration is much larger than that of the heartbeat, it is easy to observe periodic waves from the baseband output. To reject out-of-band noise and to obtain the respiration signal, a sixth-order low-pass elliptic infinite impulse response (IIR) filter was applied. The filter passes signals below 0.7 Hz and blocks those beyond 0.9 Hz. The normal heartbeat rate varies from 60 to 100 beats/min (about 1.0–1.6 Hz). To obtain the heartbeat signal, the baseband output is filtered using a seventh-order IIR filter with a passband from 0.9–9 Hz. The signals are then windowed and autocorrelated, and FFT is applied to convert to the frequency-domain response. The heartbeat rate and respiration rate are calculated in the frequency domain where FFT reaches the maximum. The detection accuracy, which is defined in [7] as the percentage of time that the measured rate is within 2% of the reference rate, was used to evaluate the detected heartbeat signals.

A. Vital Sign Measurement by a 2.4-GHz Patch Antenna

Using the setup described in the last section, the radar system was operating at 2.4 GHz with a recording time interval of 20 s. The transmitted power can be controlled through the signal generator. In this experiment, the RF output power was set at 0 dBm. It should be noted that a higher power level would extend the detection range. During the measurement, the human subject was still seated in front of the antenna and was breathing normally, in a distance of approximately 1 m.

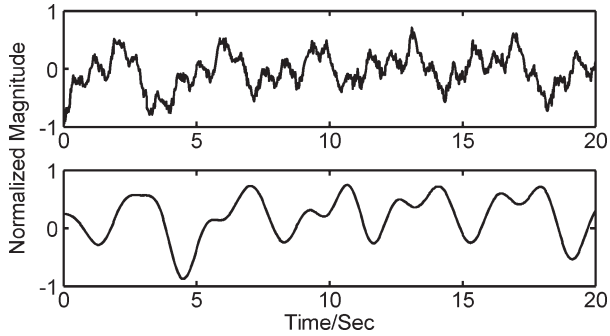

Fig. 5. Detection results. The upper trace represents the baseband output recorded by VSA software. The lower trace represents the filtered respiration signal.

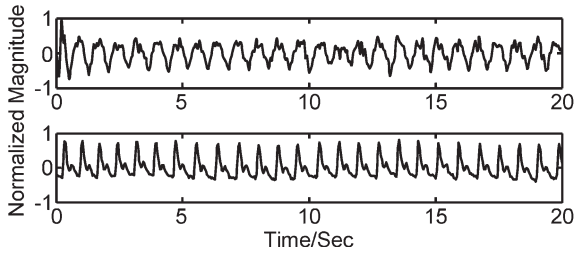

Fig. 6. Detection results. The upper trace represents the filtered heartbeat signal. The lower trace represents the reference signal.

The measurement results are presented in Figs. 5 and 6. The upper trace in Fig. 5 represents the baseband output recorded by the VSA software. This trace is rebuilt on the MATLAB platform and is known as the raw data. The lower trace represents the filtered respiration signal. It is obvious that this trace matches well with the raw trace in periodicity but is smoother than the raw trace. The upper trace in Fig. 6 represents the filtered heartbeat signal. A reference heartbeat provided by a wired sensor is shown in the lower trace. From Fig. 6, it can be seen that the detected heartbeat, which is shown as the upper trace, matches, in each pulse, with the reference heartbeat. Therefore, the detection accuracy for this measurement is 100%. By using FFT, the frequency-domain spectra of the raw data are presented as the solid line in Fig. 7. The abscissa unit

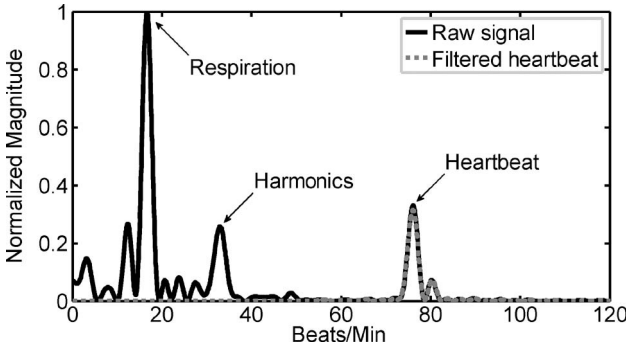

Fig. 7. Frequency spectrum of the raw signal and filtered heartbeat signal. The breathing rate is about 17 beats/min, and the heartbeat rate is about 78 beats/min.

beats per minute represents the respiration and heartbeat rates per minute. The signal amplitude is normalized. From Fig. 7, we can tell that the respiration has a much larger amplitude than the heartbeat, and it is easy to identify the harmonics of the respiration signal and heartbeat signal. The breathing and heartbeat rates are obtained by finding the peaks of respiration and heartbeat in the frequency spectrum. The breathing rate is about 17 beats/min, and the heartbeat rate is about 78 beats/min. The raw trace signal is processed to obtain the heartbeat signal, which is further processed using FFT to obtain the spectrum of heartbeat as the dashed line shown in Fig. 7.

B. Vital Sign Measurement With Variable Carrier Frequency by a 1–18-GHz Broadband Antenna

To the authors' knowledge, this instrument-based radar system is the first noncontact life-detection system that can work at a very wide frequency range from the UHF band to the K-band (20 GHz). The variable-carrier-frequency experiments were carried out in the same laboratory environment as the previous test using a patch antenna. A commercial broadband horn antenna, i.e., HD-10180DRHA, with a working bandwidth of 1.0–18.0 GHz, is used in the measurements. The measurement process is similar to the patch antenna test, except that the signal generator and the VSA software center frequency must be reset after the measurement at each carrier frequency is finished. Measurements were performed in a step of 500 MHz from 1.0 to 18.0 GHz. The MATLAB-based signal processing was applied to each measurement result to find the detection accuracy. It is found that the detection accuracy can always achieve 100% within nearly the entire frequency range if the human subject is seated at the optimal detection point. The detection accuracy decreases to 50% or less if the human subject is at the null detection point. However, for a fixed transmitted power, the amplitude of the detected vial signs varies with the carrier frequency, particularly when the frequency approaches the higher end of the frequency range. The reason is due to the increased cable attenuation, antenna mutual coupling, and higher free-space attenuation at higher frequencies. Fig. 8 shows the measured raw signals for four selected frequency points of 2.5, 7.0, 13.0, and 18.0 GHz. The corresponding frequency spectra are presented in Fig. 9.

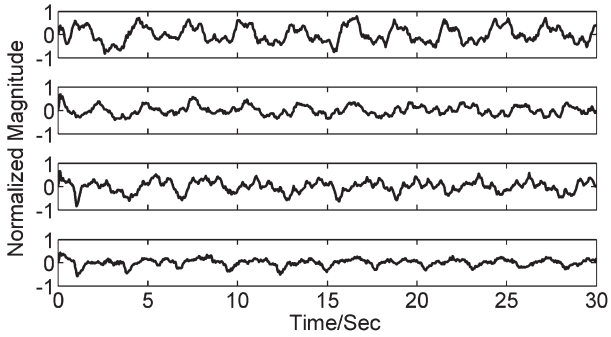

Fig. 8. Measured time-domain raw signals at four different frequency points of 2.5, 7.0, 13.0, and 18.0 GHz (from upper to lower).

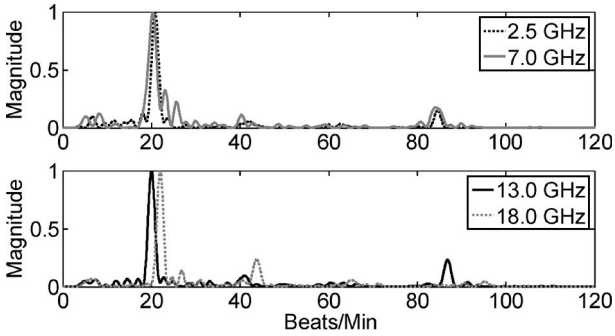

Fig. 9. Spectra of the measured raw signals at four different frequency points of 2.5, 7.0, 13.0, and 18.0 GHz.

TABLE II
SYSTEM PERFORMANCE AT DIFFERENT FREQUENCIES

Frequency [GHz]	Respiration [Beats/min]	Heartbeat [Beats/min]	Reference [Beats/min]
1.0	19	73	81
2.5	21	85	85
5.0	20	78	78
7.0	21	84	84
10.0	20	88	88
12.0	22	86	86
13.0	20	87	87
16.0	22	88	88
18.0	22	65	80

A set of data from one test is shown in Table II to illustrate the system performance within the 1–18-GHz frequency band. Each value is rounded off to the nearest integer. It is seen that the system performance goes down while approaching the edges of the frequency band.

If configured with other appropriate antennas, the system can also transmit carrier frequencies lower than 1.0 GHz. This is particularly helpful in searching survivors buried under earthquake rubbles because high-frequency radio waves have limited penetration capability. For example, an X-band system cannot sufficiently penetrate earthquake rubbles or collapsed building debris to locate the buried survivors, while L- or S-band systems can penetrate deeper [3]. The instrument-based system could work in a sweeping frequency mode to locate all possible survivors buried in various depths. Furthermore, increasing the transmitted power will increase the detection range.

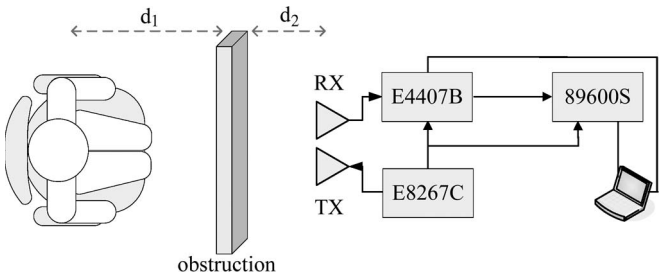

Fig. 10. Measurement setup with obstructions.

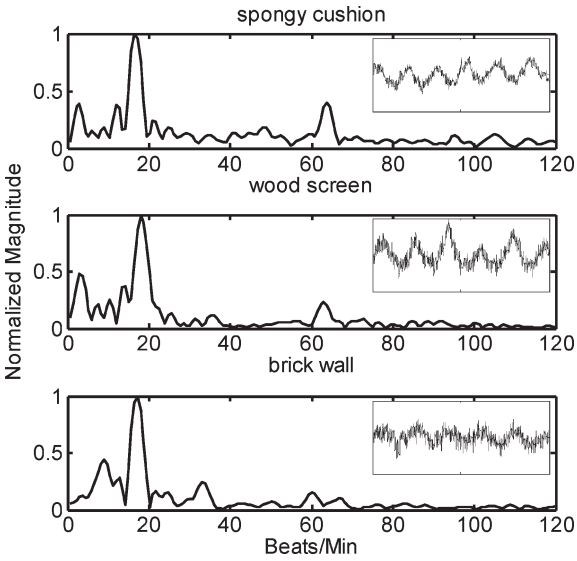

Fig. 11. Measured baseband spectra with three types of obstructions (spongy cushion, wood screen, and brick wall). The insets indicate the corresponding raw time-domain signals.

C. Vital Sign Measurement With Obstructions

Experiments were carried out with obstructions placed between the radar system and the target person. The measurement setup is shown in Fig. 10. The obstructions used in this paper were a spongy cushion (19 cm thick), a wood screen (3.7 cm thick), and a brick wall (30 cm thick). The system is configured with patch antennas, working at a fixed frequency of 2.4 GHz and a transmitted power of 0 dBm. Breathing normally, the target person was seated to face the obstruction, from a distance of d_1 away, while the radar system was placed on the other side of the obstruction, from a distance of d_2 away.

A set of experiments is carried out by varying d_1, d_2, the transmitted power, and the type of obstructions. It is found that if d_1 and d_2 are fixed, the system reaches the highest detection accuracy with the spongy cushion in between and the lowest accuracy with the brick wall. This is because the attenuation and the absorption through the brick wall are relatively higher. It is also found that the system is still able to detect vital signs even when $d_1 + d_2$ is extended to 2 m, with all the three types of obstructions. Moreover, increasing the transmitted power will improve the detection range and accuracy. The measured baseband spectra are shown in Fig. 11, where the insets indicate the raw signals. It has been demonstrated that the radar system has good performance in penetrating obstructions.

V. Conclusion

An instrument-based radar system for VSD has been presented. This radar system consists of typical microwave laboratory instruments and is easy to build. The heterodyne digital quadrature demodulation architecture alleviates I/Q imbalance and eliminates the complicated dc offset calibration. Extensive experimental verifications have been carried out using a 2.4-GHz patch antenna and a 1–18-GHz broadband antenna. It is concluded that the noncontact VSD system does not necessarily require complicated custom-designed RF circuitry. Microwave laboratories' typical instruments are sufficient to construct a Doppler radar system for measuring vital sign signals. The system is a fast solution to build a prototype to perform noncontact vital sign measurements and is expected to provide inspiration on the research of noncontact VSD.

Appendix

Assume that the transmit carrier frequency is f_1, the resulting baseband output after demodulation is

$$B_1(t) = \cos\left(\theta_1 + \frac{4\pi x(t)}{\lambda_1} + \Delta\varphi_1(t)\right) \tag{A1}$$

where $\theta_1 = 4\pi d_0/\lambda_1 + \theta_{01}$, and θ_{01} is determined by several factors such as the phase shift at the reflection surface (near 180°) and any distance between the mixer and the antenna. $\Delta\varphi_1(t)$ is the residual phase noise.

Repeating the same analysis, we have the following baseband output when the carrier frequency is f_2:

$$B_2(t) = \cos\left(\theta_2 + \frac{4\pi x(t)}{\lambda_2} + \Delta\varphi_2(t)\right). \tag{A2}$$

According to [2], when (A1) is at a null detection point

$$\theta_1 = k\pi, \qquad k = 0, \pm 1, \pm 2, \ldots. \tag{A3}$$

That is

$$\frac{4\pi d_0}{\lambda_1} + \theta_{01} = k\pi, \qquad k = 0, \pm 1, \pm 2, \ldots. \tag{A4}$$

When (A2) is at an optimum detection point

$$\frac{4\pi d_0}{\lambda_2} + \theta_{02} = k\pi + \frac{\pi}{2}, \qquad k = 0, \pm 1, \pm 2, \ldots. \tag{A5}$$

We assume that the position of the human object is fixed, which means that we have the same d_0 for both (A4) and (A5), and the carrier frequency is f_1, which happens to result in a null detection point. It is then necessary to tune the RF to reach the optimum detection point. This is achieved by tuning f_1 to f_2, i.e., (A4) to (A5). Let

$$\theta_1 - \theta_2 = \frac{4\pi d_0}{\lambda_1} - \frac{4\pi d_0}{\lambda_2} + \Delta\theta_0 = k\pi + \frac{\pi}{2}, \qquad k = 0, \pm 1, \pm 2, \ldots \tag{A6}$$

where $\Delta\theta_0 = \theta_{01} - \theta_{02}$. Substituting $\lambda_1 = c/f_1$ and $\lambda_2 = c/f_2$, the equation becomes

$$\Delta f = \frac{(2k+1)c}{8d_0} - \frac{c}{4\pi d_0}\Delta\theta_0, \qquad k = 0, \pm 1, \pm 2, \ldots \tag{A7}$$

where c is the velocity of light. Expanding (A7) leads to

$$\Delta f = \frac{75\ \text{MHz}}{d_0}(k - \partial), \qquad k = 0, \pm 1, \pm 2, \ldots \tag{A8}$$

where $\partial = \Delta\theta_0/\pi - 0.5$, which is simply an offset value.

According to the aforementioned analysis, it is demonstrated that the null detection point condition can be changed to the optimum detection point by tuning the transmit RF. For example, when the target is at 1 m away and the detection is at the null detection point, the frequency can be tuned by 75 MHz to change the null detection point to the optimum detection point.

REFERENCES

[1] J. C. Lin, "Noninvasive microwave measurement of respiration," *Proc. IEEE*, vol. 63, no. 10, p. 1530, Oct. 1975.

[2] K. M. Chen, D. Misra, H. R. Chuang, and E. Postow, "An X-band microwave life-detection system," *IEEE Trans. Biomed. Eng.*, vol. BME-33, no. 7, pp. 697–701, Jul. 1986.

[3] K. M. Chen, Y. Huang, J. Zhang, and A. Norman, "Microwave life-detection systems for searching human subjects under earthquake rubble and behind barrier," *IEEE Trans. Biomed. Eng.*, vol. 47, no. 1, pp. 105–114, Jan. 2000.

[4] B.-K. Park, O. Boric-Lubecke, and V. M. Lubecke, "Arctangent demodulation with DC offset compensation in quadrature Doppler radar receiver systems," *IEEE Trans. Microw. Theory Tech.*, vol. 55, no. 5, pp. 1073–1079, May 2007.

[5] A. D. Droitcour, O. Boric-Lubecke, V. M. Lubecke, J. Lin, and G. T. A. Kovac, "Range correlation and I/Q performance benefits in single-chip silicon Doppler radars for noncontact cardiopulmonary monitoring," *IEEE Trans. Microw. Theory Tech.*, vol. 52, no. 3, pp. 838–848, Mar. 2004.

[6] Y. Xiao, J. Lin, O. Boric-Lubecke, and V. M. Lubecke, "Frequency tuning technique for remote detection of heartbeat and respiration using low-power double-sideband transmission in Ka-band," *IEEE Trans. Microw. Theory Tech.*, vol. 54, no. 5, pp. 2023–2032, May 2006.

[7] Y. Xiao, J. Lin, O. Boric-Lubecke, and V. M. Lubecke, "A Ka-band low power Doppler radar system for remote detection of cardiopulmonary motion," in *Proc. 27th IEEE Annu. Eng. Med. Biol. Soc. Conf.*, Sep. 1–4, 2005, pp. 7151–7154.

[8] B. Lohman, O. Boric-Lubecke, V. M. Lubecke, P. W. Ong, and M. M. Sondhi, "A digital signal processor for Doppler radar sensing of vital signs," in *Proc. 23rd IEEE Annu. Eng. Med. Biol. Soc. Conf.*, 2001, vol. 4, pp. 3359–3362.

[9] B. Razavi, "Design considerations for direct-conversion receivers," *IEEE Trans. Circuits Syst. II, Analog Digit. Signal Process.*, vol. 44, no. 6, pp. 428–435, Jun. 1997.

[10] C. Li, Y. Xiao, and J. Lin, "Experiment and spectral analysis of a low-power Ka-band heartbeat detector measuring from four sides of a human body," 2*IEEE Trans. Microw. Theory Tech.*, vol. 54, no. 12, pp. 4464–4471, Dec. 2006.

[11] C. Li and J. Lin, "Optimal carrier frequency of non-contact vital sign detectors," in *Proc. IEEE Radio Wireless Symp.*, Long Beach, CA, Jan. 9–11, 2007, pp. 281–284.

[12] J. B. Y. Tsui and J. P. Stephens, Sr., "Digital microwave receiver technology," *IEEE Trans. Microw. Theory Tech.*, vol. 50, no. 3, pp. 699–705, Mar. 2002.

[13] R. Moraes and D. H. Evans, "Compensation for phase and amplitude imbalance in quadrature Doppler signals," *Ultrasound Med. Biol.*, vol. 22, no. 1, pp. 129–137, 1996.

[14] M. C. Budge, Jr. and M. P. Burt, "Range correlation effects on phase and amplitude noise," in *Proc. IEEE Southeastcon*, Charlotte, NC, 1993, p. 5.

[15] Q. Zhou, J. Liu, A. Host-Madsen, O. Boric-Lubecke, and V. Lubecke, "Detection of multiple heartbeats using Doppler radar," in *Proc. IEEE ICASSP*, May 2006, vol. 2, pp. 1160–1163.

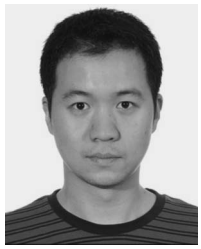

Changzhan Gu (S'07) received the B.S. and M.S. degrees in electrical engineering from Zhejiang University, Hangzhou, China, in 2006 and 2008, respectively. He is currently working toward the Ph.D. degree in electrical engineering with the Department of Electrical and Computer Engineering, University of Florida, Gainesville.

During his M.S. study, he was with the Research Laboratory of Applied Electromagnetics (AEM), Department of Information and Electronic Engineering, Zhejiang University, where he was involved in the research of UHF RFID and, later, noncontact vital sign detection, which is the topic of his M.S. thesis. His current research interests include RF circuit/system, wireless sensor, and wireless measurement technology.

Changzhi Li (S'06) received the B.S. degree in electrical engineering from Zhejiang University, Hangzhou, China, in 2004 and the Ph.D. degree in electrical engineering from the University of Florida, Gainesville, in 2009.

Since August 2009, he has been with the Department of Electrical and Computer Engineering, Texas Tech University, Lubbock, as an Assistant Professor.

Dr. Li is the second place recipient of the Best Student Paper award in the 2007 IEEE Radio and Wireless Symposium (RWS) and is a finalist in the 2008 IEEE MTT-S International Microwave Symposium (IMS) Student Paper Competition. He received IEEE MTT-S Graduate Fellowship Award in 2008.

Jenshan Lin (S'91–M'94–SM'00) received the B.S. degree from the National Chiao Tung University, Hsinchu, Taiwan, in 1987 and the M.S. and Ph.D. degrees in electrical engineering from the University of California, Los Angeles, in 1991 and 1994, respectively.

He is currently a Professor with the Department of Electrical and Computer Engineering, University of Florida, Gainesville. He is the author or a coauthor of more than 175 technical publications in refereed journals and conferences proceedings. He is the holder of seven patents. His research interests include sensors and biomedical applications of microwave and millimeter-wave technologies, wireless energy transmission, and RF system-on-chip integration.

Dr. Lin serves as an Associate Editor for the IEEE TRANSACTIONS ON MICROWAVE THEORY AND TECHNIQUES.

Jiang Long received the B.S. degree in electrical engineering in 2007 from Zhejiang University, Hangzhou, China, where he is currently working toward the M.S. degree in electrical engineering with the Department of Information and Electronic Engineering.

His current research interests include RF circuit/system, RFIC, and wireless remote phase control technology.

Jiangtao Huangfu received the B.S. and Ph.D. degrees in electrical engineering from Zhejiang University, Hangzhou, China, in 1999 and 2004, respectively.

In July 2004, he became a Lecturer with the Department of Information and Electronic Engineering, Zhejiang University, where he has been an Associate Professor since 2006. In 2007, he was with the Massachusetts Institute of Technology, Cambridge, as a Visiting Scientist for seven months. His research interests focus on RF and microwave circuits, antennas, and microwave metamaterials.

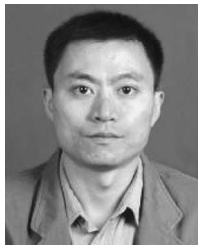

Lixin Ran received the B.S., M.S., and Ph.D. degrees from Zhejiang University, Hangzhou, China, in 1991, 1994, and 1997, respectively.

In 1999, he became an Associate Professor with the Department of Information and Electronic Engineering, Zhejiang University, where he has been a Professor since 2004. He was a Visiting Scientist with the Massachusetts Institute of Technology, Cambridge, in 2005. He is the author or a coauthor of more than 100 technical publications in refereed journals and conferences proceedings. His current research interests include RF and microwave systems, inverse scattering problems, and microwave metamaterials.